



Inkjet sensors produced by consumer printers with smartphone impedance readout

Giulio Rosati^{a,1,*}, Marco Ravarotto^a, Matteo Sanavia^a, Matteo Scaramuzza^b, Alessandro De Toni^b,
Alessandro Paccagnella^a

^a Department of Information Engineering, University of Padova, Via G. Gradenigo 6b, 35131, Padova, Italy

^b ARC, Centro Ricerche Applicate, Via J. Da Montagnana 49, 35132, Padova, Italy

ARTICLE INFO

Keywords:

EIS
Electrochemical biosensor
Impedance
Inkjet printing
Smartphone
Low-cost

ABSTRACT

Inkjet printing technology is showing a disruptive potential for low-cost optical and electrochemical biosensors fabrication. This technology is becoming affordable for every laboratory, potentially allowing every research group to implement a biosensors fabrication platform with consumer inkjet printers, commercially available inks and smartphones for readout.

In the present work we developed an example of such platform testing several inks, printers, and substrates. We defined and optimized the protocols assessing the printing limits and the fabricated biosensors electrochemical properties in standard solutions. Our platform has a total cost of less than 450 Euro and a single sensor fabrication cost of 0.026 Euro. Finally, we tested the sensitivity of smartphone-performed impedance measurements with printed biosensors surface coverage by Self Assembling Monolayers (SAM), validating them with standard instruments.

1. Introduction

The need of accurate and disposable low-cost biosensors for on-site analysis is a trend started many years ago and still ongoing. Nowadays, additional characteristics are attracting the attention of the potential biosensors users, i.e., flexibility of the devices to make them wearable, eco-compatibility of the materials, ease of use, and portability [1–4]. Few devices production techniques meet all these characteristics [5,6]. Among them, inkjet printing is one of the most outstanding since it uses an old-fashioned printing method combined with innovative nanoparticles-based inks to give relevant characteristics to the printed device, i.e., conductivity, insulating properties, hydrophobicity/hydrophilicity [7,8]. The method was even used to functionalize the printed devices with DNA-, enzyme- and antibodies-based inks. This method has been studied for the last ten years in the biosensor field, leading to a huge number of publications and interesting possibilities and applications [9–11]. However, none or few companies have started producing inkjet-printed devices for electrochemical and optical biosensing, yet.

Some of the main advantages of inkjet printing with respect to other printing techniques is that it can be used both on solid and flexible substrates [12], it requires no additional components than the inks, and

it can shorten to few minutes the time from idea to prototype [13].

Many substrates were proposed and tested in literature to be used with this technique for biosensing applications. Among them there are sustainable materials like paper, with tunable and peculiar microfluidic characteristics [14–18], and polyethylene terephthalate (PET) that is flexible, light and transparent [19–24].

The realization of easy and user-friendly measurement instruments is fundamental to implement Point of Care (PoC) system. In the last years, the smartphone use for this purpose is becoming an important trend in the biosensors field since it guarantees calculation power and internet connection [24,25]. Most of the smartphone-based biosensors make use of the smartphone camera for quantitative measurements of colorimetric reactions [26,27]. There are also some works where electrochemical biosensors are connected to small potentiostats, in turn connected to smartphones by USB or Bluetooth for analysis and data transmission [25,28–31]. However, few works were found regarding electrochemical measurements directly performed by a smartphone application [32].

In this work, we developed and characterized a simple platform for the low-cost production of inkjet-printed label-free electrochemical biosensors using consumer printers and with a commercially available

* Corresponding author.

E-mail address: giulio.rosati@icn2.cat (G. Rosati).

¹ Present address: Institut Català de Nanociència y Nanotecnologia, Edifici de la UAB 08193, Bellaterra (Barcelona), Spain.

silver nanoparticles (AgNPs) conductive ink. Then, we designed a simple biosensor for impedance measurements and we contributed to the development of a smartphone app to measure its impedance spectra in standard buffer solutions. The first commercial version of the app was intended for the characterization of electrical components such as capacitors, resistors and inductors using the smartphone as a multimeter. We collaborated with the app programmer to adapt the code for Electrochemical Impedance Spectroscopy (EIS) measurements on biosensors. Moreover, we adapted the hardware, connected to the smartphone headset plug for this application. The whole system can be easily installed and eventually customized by anyone, implementing an useful tool for PoC EIS-based electrochemical sensing and biosensing. Finally, we proved the sensitivity of the smartphone measurements to the biosensors surface by testing its coverage by different concentrations of Mercaptooundecanoic Acid (MUA) self-assembling monolayer (SAM). We performed the SAM measurements both by a standard impedance analyzer and the smartphone app, modeling the data with two specific electrical equivalent models. We found that the double layer capacitance values of the models obtained for each MUA concentration were very similar, indicating that the smartphone measurements can be used to describe the surface coverage of our biosensors, and thus for biomolecules detection. A proof of concept biosensor for antibiotic detection has already been realized with this platform [23], proving its validity in the field.

In summary, in this work we have developed and validated a low-cost platform for the fabrication of reproducible and stable electrochemical biosensors and we have introduced the first prototype of a smartphone-based PoC system for electrochemical impedance measurements, proving its validity for the investigation of molecular binding events on the biosensors surface. To our knowledge, the unique features of this platform define a very useful platform for the development of any affinity biosensor based on this technique.

2. Materials and methods

2.1. Printing materials

Two consumer printers were compared in this study, an Epson EcoTank ET-2650 and an Epson Stylus Photo 1500 W. The first has four external ink (CMYK) tanks that can be easily refilled and pipes that take the ink towards the printhead nozzles. Conversely, the Stylus printer has six internal ink cartridges directly over the printhead. Four cartridges contain the standard CMYK colors, while the other two cartridges contain lighter Cyan and Magenta for high quality shades printing. Moreover, the Stylus printer can print also over DVD sized rigid substrates. The inks used to study the printers output and to produce the sensors were the black colored inks recommended by Epson for the printers and a silver nanoparticle (AgNP) based ink from Mitsubishi Paper Mills Ltd. Japan, for home printers. The printing substrates used are divided in several types of photopaper and of PET. The photopaper brand and models are: Sigel glossy photo paper 190 g/m² and 200 g/m², Lomond 200 g/m² matte, glossy, and semiglossy bright, Epson glossy 200 g/m² and 255 g/m², and HP 200 g/m². The PET substrates brands and models are: Mitsubishi Paper Mills Ltd. Transparent PET, Lomond PET, and McDermid Autotype Autostat PET models CT5, CT7, AHU5, CUS5, CPT10L. Each substrate was purchased directly from the respective producer.

2.2. Printers preliminary tests

Prior to use the consumer printers to produce electrochemical sensors, the use of inks with different properties is necessary, e.g. AgNP and AuNP conductive inks for contacts and electrodes, and insulating inks for passivation of the parts not to be contacted by the testing solution. For this reason, we set a protocol for inks loading and substitution to avoid any contamination with previous inks within the

printers. With the same goal, the possible cross-contaminations between the inks were assessed for both printers and relative printing software parameters. Finally, the stability and printability of the inks after their injection in the printers were evaluated. The cross-contaminations of the inks is a typical problem of consumer inkjet printers, since, differently from research-grade printers, they can contain and print more than one ink at a time. In fact, in this case cross-contaminations are defined as the printing of a pattern by more than one ink at a time and is generally due to built-in printers settings conceived to optimize the print quality of the colors or to save ink. For example, with some office printers, if not differently specified, the black designs can be printed mixing the cyan, magenta and yellow inks instead of using the black one.

Finally, we tested the ink drying on the substrate at room temperature right after printing. This is possible only if the substrate has an adsorbing surface. Avoiding any annealing or sintering steps simplify the sensors fabrication procedure.

2.2.1. Inks substitution protocol

Substitution of the inks is necessary when the cartridge/tank is finished, and when the users need to use a different type of ink in the same color channel. However, consumer printers are not designed to support different types of ink in the same color channel. For this reason, it has been necessary to study a protocol to change the printer components that come in contact with the ink each time it is finished or it has to be changed. At the beginning we consider to simply use empty cartridges and flushing the ink to remove the traces of the previous one. However, this strategy wastes a high volume of ink and after the first tests we proved that traces of the previous ink were still present after flushing the new one. Therefore, we studied the ink path in the printer with a reverse engineering process. Fig. A1 describes the inks flow from the respective reservoirs to the waste collectors, along with the printers' mechanical and hydraulic parts in contact with them. We found the corresponding parts commercially available and we defined a protocol to substitute them to avoid contaminations between former and new inks in the same color channels.

2.2.2. Cross-contaminations assessment

To assess the possible cross-contamination during printing, we designed a simple five colors layout in AutoCAD 2016™ by setting the cyan, magenta, yellow and black (CMYK) colors directly by their RGB codes. Then, we printed the same layout several times, blocking with adhesive tape the single colors nozzles' lines. The printed bands allowed the identification of the cross-contaminations, e.g., if the black band is printed even with the black nozzles blocked by the tape it means that other channels participate in its printing. An example of the layout and of the printing results is reported in Fig. A2. Since color management depends on the selected substrate type when printing an image, we repeated the tests for all the substrate types present in the printer management software.

2.2.3. Ink drying on the substrates

Since thermal annealing and sintering protocols are often time consuming and require specific instrumentations, we looked for substrates with absorption/capture layers capable to filter the AgNPs ink on their surface from the ink solvents. In this way, the printed layout is almost immediately dried and conductive. For this test we printed filled squares with AgNP ink on all the substrates, and we tested the ink by gently brush the squares with absorbing towels and cotton swabs 10 min after printing. During these 10 min, the substrates were kept in unsealed Petri dishes at room temperature with humidity ranging between 30% and 50%.

2.3. Printers resolution tests

The resolution of inkjet consumer printers depends on: software

parameters and limitations, printer mechanical characteristics, and substrate/ink properties and interaction. Each one of the previous elements introduces a quantization on the rasterization of the image, as depicted in Fig. B1. Moreover, consumer printers usually have different mechanisms to move the printhead along the x and y directions. Consequently, different resolutions should be expected along the two axis (Q2x and Q2y in Fig. B1).

By using AutoCAD 2016, the software rasterization resolution Q1 is known since the software printing resolution is 720 dpi and this means a rasterization with a $35.28\ \mu\text{m}$ step. Regarding Q2x and Q2y, we designed a layout composed by vertical and horizontal lines, considering as horizontal the printhead movement direction. All the lines were 2 cm long and they were characterized by widths calculated to be quantized by the software (Q1) in the same way, i.e., two by two, as depicted in Fig. B2.

The design was printed with AgNP ink on Sigel glossy photopaper $190\ \text{g}/\text{cm}^2$ and the lines widths were measured by transmission microphotography with a Leica DM-LB2 microscope, a Nikon Coolpix 4500 camera and a custom built Matlab function validated on Edmund Optics NASAF targets for microscopes resolution testing [33].

2.4. Spatial reproducibility

Since the printhead movement takes place sliding along a metal guide, the horizontal lines are always more resolved than the vertical ones, which are produced by few ink drops for each printhead transition over the printing area, during the substrate progression under it. Therefore, we designed a new layout reproducing the horizontal lines of Fig. B2 all over the surface of an A4 Sigel glossy photopaper $190\ \text{g}/\text{m}^2$ sheet. Then, we measured the width of the printed lines to assess their spatial reproducibility over the substrate area.

2.5. Selected substrates comparison

The substrates that passed the drying test described in paragraph 2.2.3 were further characterized by printing a layout with 2 cm long lines and widths ranging from 100 to $800\ \mu\text{m}$ with a $100\ \mu\text{m}$ step plus a $50\ \mu\text{m}$ wide line. The printed devices were tested for:

- *Width bias*: the difference between the measured and nominal width, the former being characterized by microphotographs and MatLab elaboration as previously explained in paragraph 2.3.
- *Sheet resistance*: the resistance of each printed line was tested by an Agilent U1241B multimeter and the corresponding sheet resistance was calculated by multiplying the resistance by the ratio between the lines length and their measured width.
- *Stability after printing*: the devices' resistances were measured 1, 24, 48, 72, and 96 h after printing. The time after which the sheet resistance remained unchanged was considered as the stabilization time of the device.
- *Adhesion*: the AgNP printed lines adhesion over the substrates was characterized by a peeling test.

2.6. Sensors passivation

To passivate the sensor contacts we decided not to use inkjet printing because this would require another passage in the printer with possible alignment problems and also because the ink composition could alter the electrochemical properties of the devices. Therefore, we decided to use a CraftRobo CC330 automatic cutter with RoboMaster software to pattern vinyl adhesive sheets (by Tosigraf, Vicenza, Italy) and GBC plastic pouches ($125\ \mu\text{m}$) to be put over the printed devices. Moreover, we compared the cutting resolution, the contact angle, and the resistance of the passivating membranes to the exposition to 99.8% ethanol overnight, which is a common protocol for electrochemical devices functionalization with SAMs. The contact angle measurements

were performed dropping 5 drops of $5\ \mu\text{l}$ on the substrate on a flat horizontal stage and taking pictures right after the dropcasting with a high resolution Thorlabs camera. The measurements were performed in a dark box with the same illumination source. For vinyl cutting, we fixed the vinyl sheet to normal cardboard to give it more rigidity and we adopted the respective default parameters of the RoboMaster software for this specific application. Conversely, to pattern just one of the plastic pouches sides, we fixed them on cardboard with biadhesive tape. Then, we designed a cutting layout with horizontal and vertical bands of different widths, and with squares and circles of dimensions ranging from 0.1 mm to 30 mm. Finally, we compared the cutting precision before and after the application of the membranes on the substrate.

2.7. Sensors layout and impedance measurements

Once selected the passivation method, we designed a layout for EIS-based sensors, with two parallel $400\ \mu\text{m}$ wide electrodes with a $400\ \mu\text{m}$ gap and a 2 mm wide and 3 mm high active window, as depicted in Fig. C1c. Then, we replicated it on an A5 sheet adding a control area with lines of known resistance values (Fig. C1a), and we patterned plastic pouches for insulation (Fig. C1b and C1d). Finally, we cut the single sensors and we connected them to a custom PCB for the EIS measurements with a testing solution volume of $25\ \mu\text{l}$. The solutions used for the tests were 10 mM Phosphate Buffered Saline (PBS) from Sigma-Aldrich, prepared from pre-weighted powder pouches in MilliQ ultrapure water ($18.2\ \text{M}\Omega\ \text{cm}$), and Potassium Phosphate Buffer (PPB) prepared by dissolving monobasic and dibasic potassium phosphate (Sigma-Aldrich) in milliQ water to obtain pH 7.4.

We performed the EIS measurements to test the sensors impedance response with 0 V DC and 10 mV peak-to-peak AC voltage in a frequency range between 100 mHz and 1 MHz with a Solartron 1260 impedance analyzer connected to the PCB by BNC wires.

The smartphone impedance measurements were performed by the optimized application, which can be found in Google Play [34], and a custom PCB circuit connected to the smartphone by the headset plug (Fig. C2 (c)). The circuit scheme is incorporated in the application and we added a flat ribbon connector to contact the sensor's electrodes and a sealed case to prevent the hardware to come in contact with the solutions tested by the sensors.

The measurements were performed with 0 V DC and 10 mV AC at frequencies ranging between 50 Hz and 20 kHz, which is the broadest frequency range possible with this system. An example of the app running the measurements is provided in Fig. C2 (a), with a magnification of one of the devices (Fig. 2 (b)).

To assess the application validity for the impedance measurements on the sensors we performed two measurements on the same sensor in PBS, first with the Solartron 1260 impedance analyzer and then with the smartphone readout. For this test, we set the DC voltage to 0 V, the AC voltage to 10 mV, and we collected the data at 50, 100, 200, 500, 1 k, 2 k, 5 k, 10 k, 20 kHz.

2.8. Sensors functionalization

With the aim to test the sensors functionalization, we immobilized a Self-Assembling Monolayer of Mercaptoundecanoic Acid (MUA) by immersion in Ethanol overnight at $4\ ^\circ\text{C}$. We tested MUA concentrations ranging from $1\ \mu\text{M}$ to 10 mM and then we measured the EIS response of the sensors both by Solartron 1260 impedance analyzer and by the smartphone LCR meter app. Finally, we defined two electrical equivalent models to fit the collected EIS data and we compared the resulting double layer capacitance values.

3. Results and discussion

3.1. Printers preliminary tests

The preliminary activities for the sensors production consisted in the technical analysis of the Epson ET-2650 and Stylus 1500 W models, with the goal of comparing an external tank printer with a cartridge-based one (Fig. A1). The in-depth analysis of the printers allowed also to define the parts that should be changed to guarantee no contaminations upon inks changing operations. The study showed that the Stylus cartridge-based model allowed to save a huge ink quantity with respect to the tank-based ET-2650 model. In fact, the distance between the ink tanks and the printhead in the ET-2650 model imply that at least 13 ml of ink are dispersed in the connecting pipes. Conversely, in the Stylus model the 11 ml cartridges are placed directly over the printhead. The most effective inks substitution protocol we found consists in the change of the cartridge, the printhead, and the cleaning sponges. The protocol is in line with what is normally done with research-grade inkjet printers such as Dimatix 2800 and 2831 and, even if expensive, results the most effective.

After this analysis we tested the cross-contaminations between inks, using the native colored printer inks and a simple AutoCAD design with different printing parameters. ET-2650 model resulted more robust, with only one cross-contamination in the black channel with the Glossy paper type configuration.

Conversely, Stylus 1500 W showed many cross-contaminations with most of the paper type configurations. The only channel unaffected by cross-contaminations were black and yellow with common, premium glossy and quality inkjet paper types. Despite these results, we decided to use the Stylus model for the following tests because it has lower ink consumption and easier ink substitution protocols than the ET-2650 model. For this reason, we adopted the Stylus model printer with the following printing settings: no color adjustment, best photo quality, premium glossy paper and all other settings set to off.

In order to test the inks stability in the selected printer, i.e., their printability days after the inks loading in the cartridges, we performed a nozzle check (a printer built in function to check the status of each single nozzle of the printhead) every day for two weeks. In case of clogging of more than 5% of the nozzle we started the built-in procedure for printhead cleaning and we performed the nozzle check again. Among the commercially available inks, we chose the one with the best cost/quantity ratio, which did not clog the printhead nozzles over the two weeks of tests. The ink is based on silver nanoparticles (AgNP) and is sold by Mitsubishi Paper Mills Ltd. Therefore, we loaded only the

AgNP and the black inks in the Stylus channels not affected by cross-contaminations.

Another ink showed promising results (Novacentrix), but in that case the nozzles were free only after a cleaning procedure that is expensive in terms of wasted ink.

We preliminary tested 15 different plastic and paper-based substrates to assess which of them could guarantee the ink drying 10 min after printing. This feature is important when printing with a 1-axis printers (instead of 2-axis, i.e., plotters). In fact, if the ink does not dry fast enough the substrate movement inside the printer could create undesired defects. This is mainly due to the substrate movement inside the printer. For instance, research-grade printers always have a flat stage where the substrate is standing still perfectly horizontal, and a printhead that moves in 2 dimensions with respect to it. In this way, the ink jetted on the substrate does not face any kind of acceleration and remain where deposited. Conversely, consumer printers always have a single axis printhead and the second degree of freedom is defined moving the substrate that is also tilted at different angles during the print. From here, the preferential choice of an absorbing coating on the substrate using this type of printers. Moreover, these coatings have further advantages. Often, they filter the nanoparticles on the surface, up-concentrating them, and allowing to obtain lower resistances of the printed patterns. In some cases, as for Mitsubishi's substrates, the coatings also contain nanoparticles coming in contact with the AgNPs by osmosis through the ink solvent jetted on the absorbing coating. These nanoparticles are specifically designed to remove the AgNP shells preventing agglomeration in solution, further increasing the conductance between the printed AgNP. This process is commonly known as chemical sintering.

The results of the ink drying test are reported in Tab. A1 in Appendix. Only six substrates (indicated in bold in Tab. A1) were suitable for further tests with printed AgNP ink, as can be seen in paragraph 2.4. The unselected substrates characterized by ink drying showed rougher surfaces or no conductivity of the printed AgNP ink.

3.2. Printer resolution

The printer resolution is a challenging issue when using consumer 1-axis printers. As represented in Fig. B1, the resolution is influenced by the following aspects: the layout design software; the printing settings; the printer mechanical characteristics; the substrate properties. We assessed the contribution of each of this factor by printing horizontal and vertical lines with respect to the printhead movement direction. The length of the lines was 2 cm, while the widths were calculated from

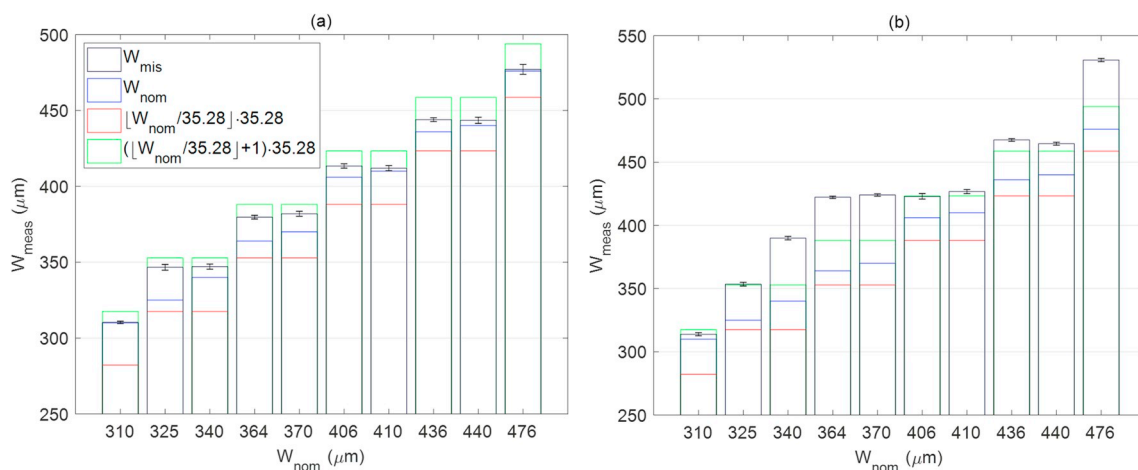


Fig. 1. Comparison between measured and nominal widths of lines printed in the printhead's movement direction (a) and in the perpendicular direction (b). The black bar represents the average width and its standard deviation, the green and red bars represent the lower and upper dimensions with a quantum step of 35.28 μm . The blue bar represents the nominal width value.

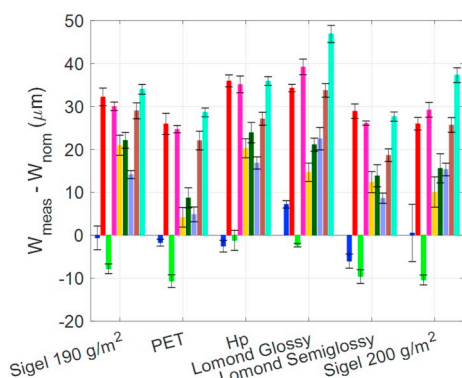


Fig. 2. Average difference between measured and nominal widths of lines printed in the printhead's movement direction on the selected substrates, for width of 50, and 100–800 μm with a step of 100 μm (as indicated by the colors, from left to right).

the known layout design software resolution, i.e., 35 $\mu\text{m}/\text{pixel}$ (Fig. B2). The study of the printer resolution, both in the printhead movement direction and perpendicularly to it, gave the results depicted in Fig. 1a and b, respectively. The plots show the average measured width (with a custom Matlab function [35]) and the respective standard deviations (in black), as a function of the nominal lines width, which is also represented by the blue lines. The red and green lines in the bars represent the floor and ceiling calculated values for each nominal width, reported in Fig. B2.

As can be seen in Fig. 1a, the measured width (in black) always lie between the calculated floor (in red) and ceiling (in green) values. Moreover, the measured width is stair shaped, with an average step amplitude of 35 μm .

The situation in Fig. 1b is completely different: only two measured widths lie within the calculated floor and ceiling values and the stair shape is not present at all. In particular, between 364 and 410 μm the measured widths are identical, while for thinner or thicker lines the measured widths are much different. Only horizontal lines can be printed with exact widths and this is very important for many sensors layouts, e.g. interdigitated sensors. Therefore, we decided to use only horizontal lines for sensors electrodes printing and vertical lines for contacts and other non-critical parts.

3.3. Spatial reproducibility

The spatial reproducibility study along the height of the A4 sheet was performed on 15 lines printed along the printhead movement direction, as detailed in paragraph 2.4. The percentage variations of the measured widths with respect to the nominal values were calculated by the following equation:

$$\Delta W = 100(W_{\text{meas}} - W_{\text{nom}})/W_{\text{nom}} \quad (1)$$

The obtained matrix of values is depicted in the contour plot of Fig. B3b, next to the image of the printed A4 sheet. Despite the maximum variations were beneath 15%, the contour plot evidences a periodicity of the variations of the measured widths with respect to the nominal ones. In fact, the values close to zero lie in four zones separated by 10 cm on the Y axis.

3.4. Selected substrates comparison

In this part of the work, we characterized the six substrates selected after the previous tests. We printed devices made by horizontal lines of different widths on each substrate. As described in paragraph 2.5, the six selected substrates were tested in terms of the obtained resolution, the sheet resistance of the AgNP printed lines, the stability of the resistance over time, and the ink adhesion. Fig. B4 shows reflection

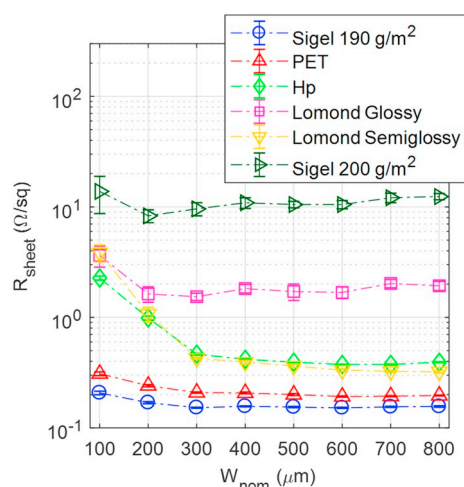


Fig. 3. Sheet resistance of the lines printed on the selected substrates as a function of the nominal lines' width (the 50 μm lines are excluded because two samples over five were not conductive). The R_{sheet} values were obtained after stabilization for each substrate (hours after printing indicated between square brackets in legend).

micrographs of 400 μm wide lines on the selected substrates.

In Fig. 2, we plot the differences between the measured and nominal widths of the lines printed on each substrate, represented on the x axis. The colored bars described in the legend refer to the different nominal widths of the printed lines.

The differences between the real and nominal widths resulted lower than the software resolution in all cases except for Lomond Glossy (Fig. 2). Mitsubishi PET and Lomond Semiglossy are the substrates that showed the lowest differences. The devices sheet resistance was calculated from both electrical resistance measurements and lines geometrical features for each substrate (Fig. 3).

Lomond glossy and Sigel 200 g/m² showed the highest sheet resistance values. Conversely, Mitsubishi PET and Sigel 190 g/m² presented the best results.

Except the thinnest lines, the sheet resistances are independent from the lines' width. The changes of the sheet resistance values for the thinnest lines is probably due to the impact of the printing defects, that becomes more relevant as the line width approaches the software resolution. For instance, the Lomond and HP substrates, showed an important increase of the sheet resistance for lines thinner than 300 μm . This may be due to the porosity of the substrate coating, observed to be higher than those ones of the other substrates, and thus not able to accumulate the AgNPs in the printed ink when its volume is less than a certain quantity.

Regarding the stability, the lines resistances were tested for 5 days, once per day, after printing. The stability of the response has been defined as the number of hours after which the measurements lie in the respective standard deviations (Tab. A2 in Appendix). The substrate that require the lowest amount of time to stabilize resulted Mitsubishi PET, Lomond Glossy and Sigel 200 g/m². The storage stability of the devices was tested too. The comparison of storage of the devices at different temperatures, i.e., RT, 4 $^{\circ}\text{C}$ and -20°C , and different containers, i.e., sealed plastic bags, vacuum bags and unsealed Petri dishes showed very interesting results. In fact, the devices that result more stable where those ones stored at 4 $^{\circ}\text{C}$ in sealed bags, with resistances remaining almost constant for at least 3 weeks.

The adhesion of the ink to each substrate was tested by a simple peeling test, which showed excellent results, i.e., no detachment of the printed lines, only for Mitsubishi PET and Sigel 200 g/m².

The results obtained by these tests and characterizations pointed out Mitsubishi PET as the most performing substrate for devices printing. Therefore, this substrate was selected for the following

characterizations.

3.5. Sensors passivation

We compared the results of two devices insulation methods, i.e., adhesive and thermal lamination: in the former, a patterned polymeric patch made of adhesive vinyl is placed on the printed devices, while in the latter a plastic pouch is bonded around the devices by thermal lamination. As detailed in paragraph 2.6, we used a cutting plotter to pattern the materials and we defined a layout to define the cutting resolution, which depends also on the materials mechanical properties. Moreover, we measured the materials contact angle with water droplets. The hydrophobicity of the passivation membrane is an important property for electrochemical biosensors, since it's fundamental to keep the liquid sample to analyze on the electrodes. Most of the sample in fact are water-based, and a hydrophobic insulating layer defining the electrodes-solution contact area and keeping the solution drop stable, is highly desirable.

The results of the layout patterning were compared in terms of the actual size of the short side of the vertical and horizontal rectangles. These were measured from the reflectance micrographs of the samples before and after their application on a colored testing substrate. Fig. 4 represent the comparison between the measurements. Fig. 4 inset shows the differences between these values and the nominal ones.

The contact angle average values with standard deviations were $82^\circ \pm 2^\circ$, $74^\circ \pm 2^\circ$, and $79^\circ \pm 5^\circ$ for vinyl, a plastic pouch, and Mitsubishi PET, respectively. All these values result suitable for bio-sensing purposes and in line with the values that can be obtained on commercial sensors, such as DropSens screen printed electrodes.

The two passivation methods led to very similar results in terms of patterned dimension differences and contact angles, but the thermal bonding with plastic pouches can be easily scaled up in a manufacturing process with plasticization machines, which assures uniform pressure and temperature. For these reasons this kind of passivation has been adopted for the printed devices.

3.6. Sensors layout and impedance measurements

In this part, we defined a simple layout for our electrochemical printed sensor and for the respective passivation, depicted in Fig. C1. The sensors were printed on Mitsubishi PET with AgNP ink and passivated by patterned plastic pouch. Three devices were then measured by EIS in PBS and three in PPB by the impedance analyzer. Despite their different response in the Bode's diagram (Fig. 5), they can be both modeled by the well-known Randles model (in the inset of Fig. 5),

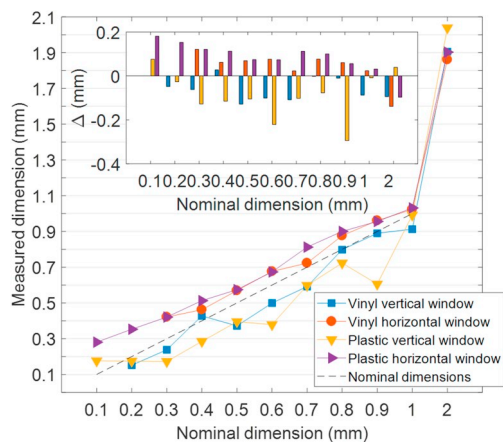


Fig. 4. Measured dimensions of the vertical and horizontal bars on the patterned vinyl and plastic pouch. The inset shows the differences between the measurements and the nominal values.

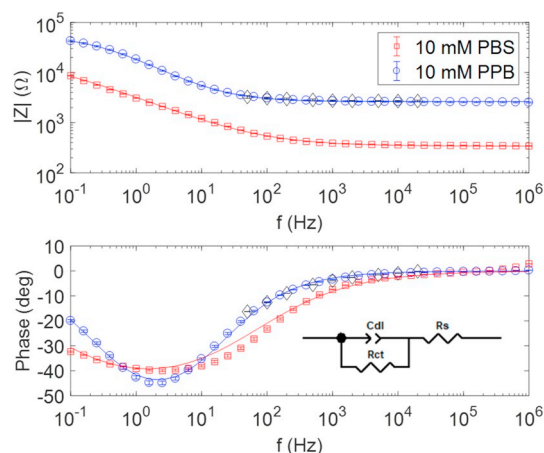


Fig. 5. Bode diagram of the measurements performed on PET printed sensor in 10 mM PBS and 10 mM PPB by the Solartron 1260 impedance analyzer and respective fits by the Randles cell reported in the inset. The black diamond markers represent the measurements performed by smartphone on the same sensors in 10 mM PPB.

Table 1

Randles cell fit values for 10 mM PBS and 10 mM PPB on the printed sensors.

Buffer	χ^2 ()	R_s (Ω)	C_{dl} (μF)	n ()	R_{ct} (k Ω)
PBS	0.0045	340 ± 3	111.05 ± 2.72	0.55 ± 0.01	20.34 ± 1.49
PPB	0.0015	2622 ± 8	13.69 ± 0.14	0.71 ± 0.01	52.87 ± 0.64

obtaining the fit results depicted in Table 1.

Moreover, in order to compare the impedance analyzer and the smartphone measurements, we measured the same number of devices in PPB also with the smartphone app. The data obtained are plotted in Fig. 5 (black diamonds).

Even though the smartphone app frequency range is limited between 50 Hz and 20 kHz (the range of the audio signals recording by the smartphone microphone) the measurements overlap with those performed with the Solartron 1260 impedance analyzer.

As can be seen, the goodness of fit is higher for PPB than for PBS data, thus we decided to use this buffer solution for the following functionalization experiments, described in paragraph 2.8.

To test the sensitivity of the impedance spectra measured by smartphone to the sensors surface coverage, we used different MUA dilutions in pure ethanol to functionalize the electrodes surface. The binding of MUA to the AgNPs took place thanks to the MUA terminal thiols groups. Generally, the coverage of the sensors' surface, i.e., their functionalization and the target binding to the probes molecules, can be easily monitored by both the charge transfer resistance and double layer capacitance changes [35,36]. Therefore, in Fig. 6 we compared the double layer capacitance values obtained by the fit of the Solartron 1260 measurements by the Randles model, and the values obtained from the smartphone measurements obtained by the R-CPE series model (depicted in the inset of Fig. 6). The EIS spectra reported in the inset are plotted without the standard deviation bars to avoid confusing the reader and because the Zview fitting software does not weight the data with the standard deviations. However, the calculated coefficient of variations for the data points were always lower than 4% with just one point resulting with a 5.3% value.

The use of a different model for the smartphone measurements was necessary since the frequency range allowed to observe just the contribution of the solution resistance (R_s) and of the double layer capacitance (C_{dl}). The resulting C_{dl} values are compared to those obtained by the smartphone measurements fit in Fig. 6.

Fig. 6 proves that the sensors with this layout can be successfully measured by smartphone to define their surface coverage. Therefore,

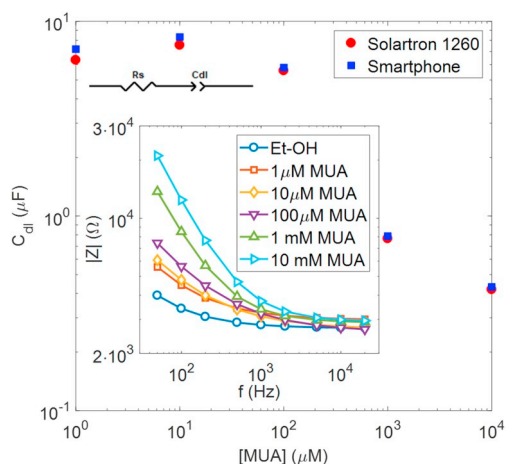


Fig. 6. Double layer capacitance values obtained by the fits with the electrical equivalent model reported in the Figure. The smartphone measurements performed with different MUA dilutions are showed in the inset. The points represent the average values (the deviations were removed to keep the plot clear) and the curves represent the obtained fits.

our printed sensors can be used for impedimetric affinity detection in antibodies- or aptamers-based systems.

3.7. Sensors inkjet printing platform costs

In this paper, we wish to propose a reliable low-cost platform for the fabrication of electrochemical biosensors that can be measured by smartphone. The devices are disposable and ecofriendly. The fixed costs total is 425 €. Since an A5 sheet can contain up to 160 sensors, and

Appendices

Appendix A. Printers preliminary tests

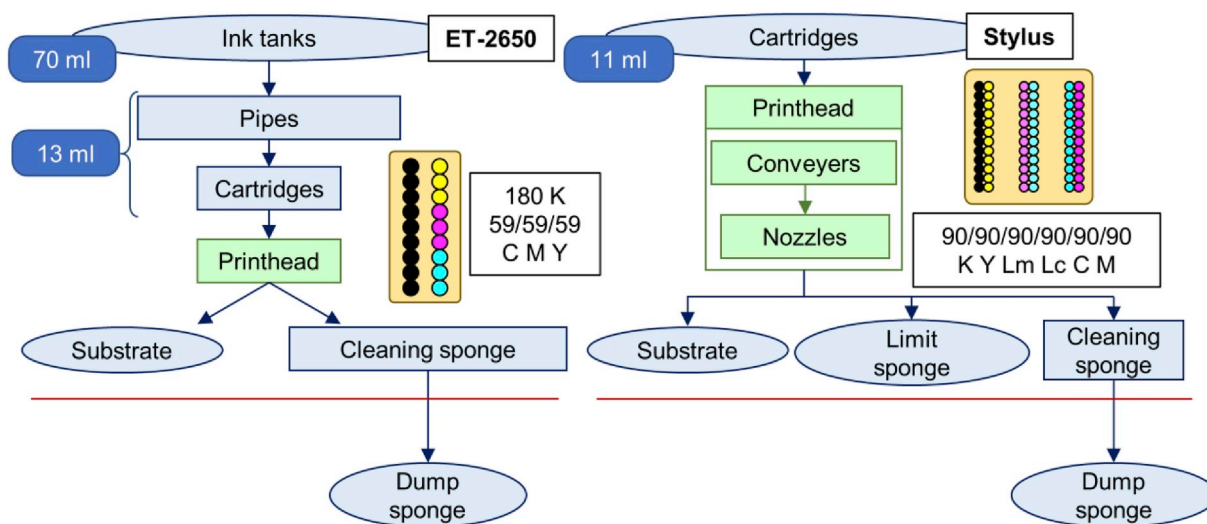


Fig. A1. Representation of the printers' parts that come in contact with the inks in the ET-2650 and the Stylus printers. The blue boxes show the capacity of each ink tanks/cartridges, and the approximated ink volume dispersed between them and the printheads. A schematic representation of the nozzles disposition on the printheads is also shown with the number of nozzles available for each ink channel.

100 ml of AgNP ink allow to print about 200 sheets, the variable costs can be calculated as 0.026 €/sensor. With these costs, every laboratory and even every person who is interested in these topics can start a sensors production platform that enables for an ultra-short concept to prototype time. In this way, the time requested for the realization of a complete biosensors depends only on its surface functionalization.

4. Conclusions

In this work we presented the development of a low-cost platform for inkjet-printed biosensors fabrication on flexible substrates. With a total cost of 425 € it is possible to produce electrochemical affinity impedance-based biosensors with a cost of 0.026 €/sensor, excluding only the functionalization that depends on the specific target to be detected.

We analyzed both the inks, the consumer printers, and the substrates that allow to obtain the highest resolution, reproducibility and performance for the devices fabrication. Then, we found a method for their passivation and we tested their impedance response with two common buffers. We proved their sensitivity to surface coverage using a well-known SAM, and finally we tested them with a smartphone impedimetric readout by a commercial application.

These results allow everyone to setup a low-cost and easy-to-use biosensor fabrication platform for use in many fields with a POC approach, ranging from medicine to food control [24].

Conflicts of interest

The following authors have no financial disclosures: RG, MR, MS, MS, ADT, AP.

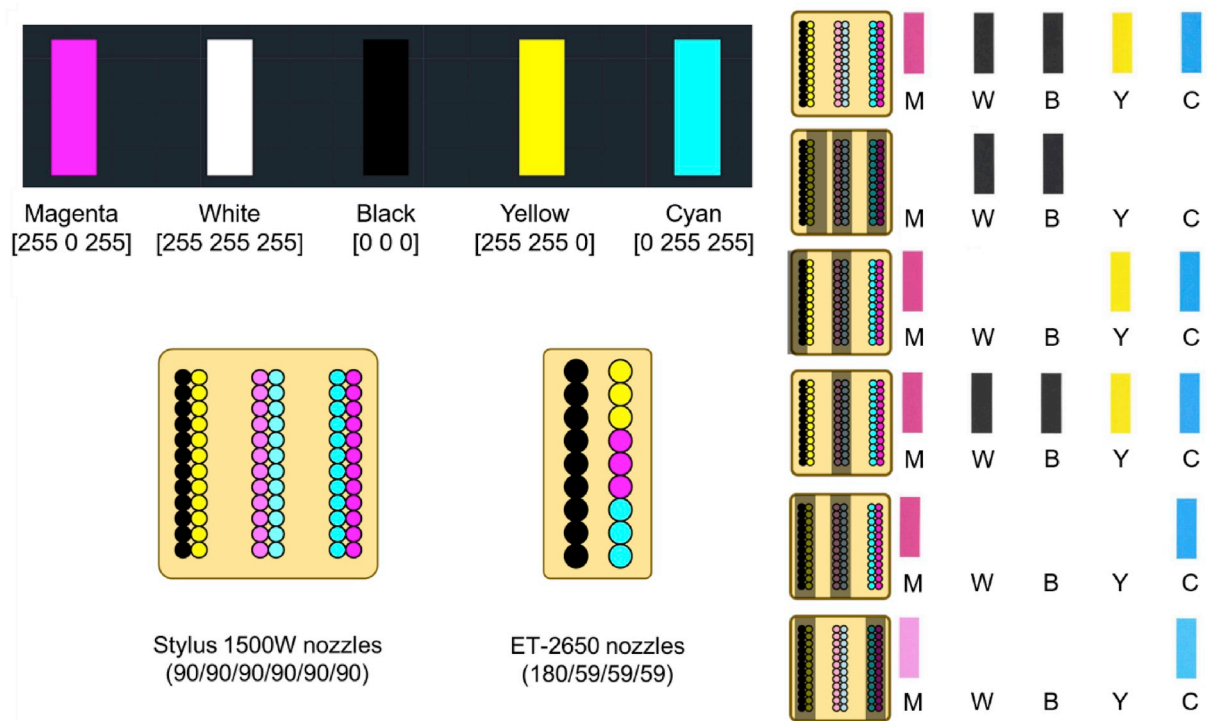


Fig. A2. AutoCAD layout used for the cross-contamination tests (top left corner), Stylus and ET-2650 printheads nozzles schemes (bottom left corner), and example of the cross-contamination test results obtained blocking the nozzles as indicated in the Fig. (right).

Tab. A1

Epson Stylus 1500W drying substrate test result 10 min after printing. Coated means that the substrate has an absorbing layer on that side of the sheet.

Substrate	Sheet side	Results	Substrate	Sheet side	Results
Sigel 190 g/m2	Front (coated)	Dry	Mitsubishi PET	Front (coated)	Dry
	Back (uncoated)	Wet		Back (uncoated)	Wet
Sigel 200 g/m2	Front (coated)	Dry	Lomond PET	Front (coated)	Dry
	Back (uncoated)	Wet		Back (uncoated)	Wet
HP 200 g/m2	Front (coated)	Dry	Autotype PET CT5	Front (coated)	Wet
	Back (uncoated)	Wet		Back (coated)	Wet
Lomond Matte	Front (coated)	Dry	Autotype PET CT7	Front (coated)	Wet
	Back (coated)	Dry		Back (coated)	Wet
Lomond glossy	Front (coated)	Dry	Autotype PET AHU5	Front (uncoated)	Wet
	Back (uncoated)	Dry		Back (uncoated)	Wet
Lomond Semiglossy	Front (coated)	Dry	Autotype PET CUS5	Front (coated)	Wet
	Back (uncoated)	Wet		Back (coated)	Wet
Epson 200	Front (coated)	Dry	Autotype PET CPT10L	Front (coated)	Wet
	Back (uncoated)	Wet		Back (coated)	Wet
Epson 225	Front (coated)	Dry			
	Back (uncoated)	Wet			

Tab. A2

Average hours needed for the stabilization of the resistance values of the printed lines for the selected substrates.

W_{nom}	Sigel 190	Mitsubishi PET	HP 200	Lomond Glossy	Lomond Semiglossy	Sigel 200
50	24	96	96	96	96	96
100	72	48	72	1	72	24
200	72	48	72	1	72	48
300	72	48	96	24	96	24
400	24	1	96	1	96	1
500	24	1	96	1	96	24
600	24	24	96	24	96	48
700	24	24	96	24	96	24
800	72	24	96	24	96	24

Appendix B. Printer resolution and spatial reproducibility

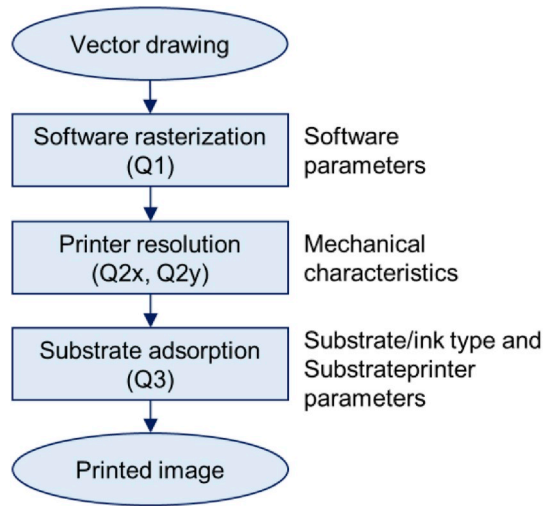




Fig. B1. Schematization of the single contribution to the printed image resolution. Sigel glossy photopaper 190 g/m² was selected for the following printers' tests since it enabled a faster inks drying than other substrates.

Lines width (µm)	310	325	340	364	370	406	410	436	440	476
Q1 floor	282,24	317,52	317,52	352,8	352,8	388,08	388,08	423,36	423,36	458,64
Q1 ceiling	317,52	352,8	352,8	388,08	388,08	423,36	423,36	458,64	458,64	493,92

Horizontal lines 

Vertical lines 

Lines width (µm) 310 325 340 364 370 406 410 436 440 476

Fig. B2. Distribution of the test line widths and respective calculated floor and ceiling quantized width values on the basis of the software minimal step of 35.28 µm (Q1).

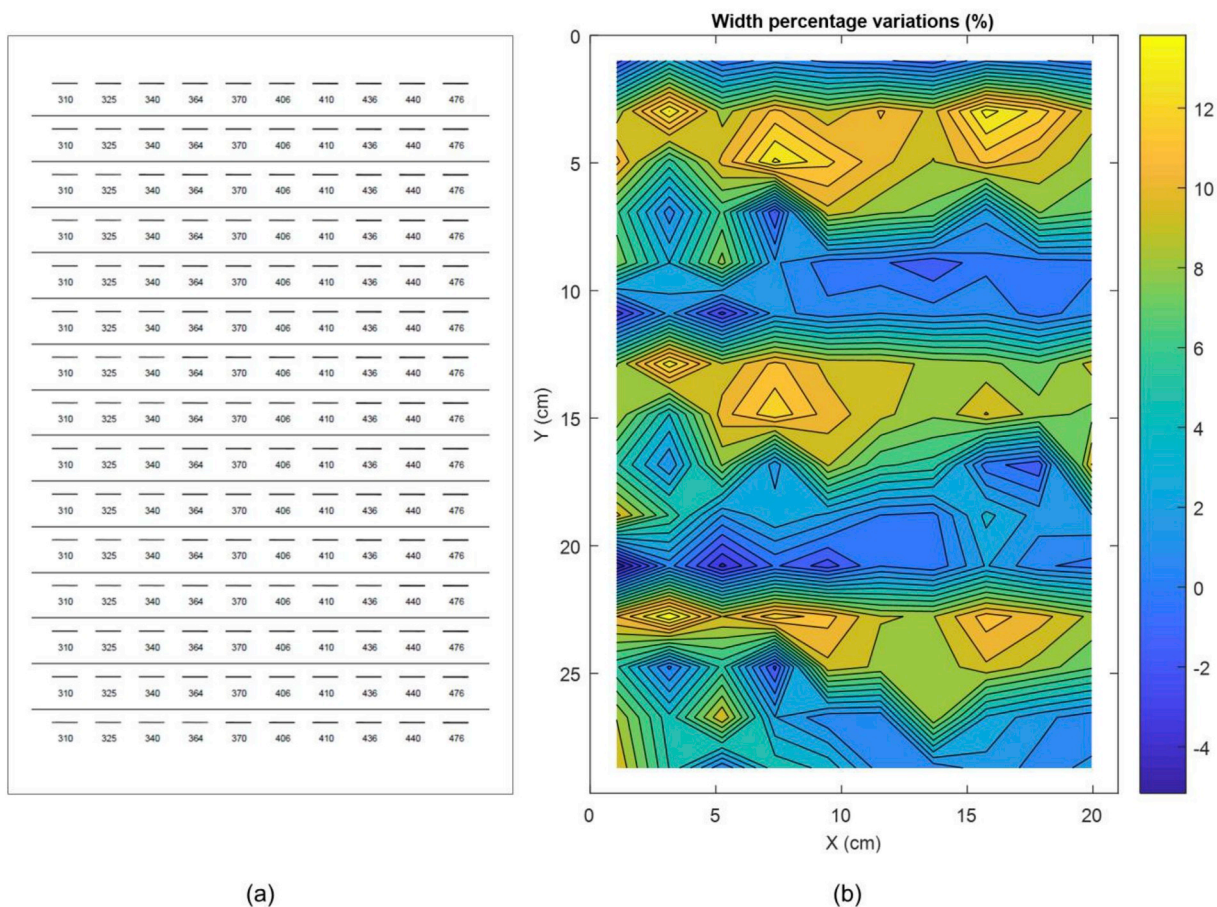


Fig. B3. (a) Printed A4 sheet for the spatial uniformity test. The test lines are printed in the printhead movement direction with the same widths of the previous test; (b) Contour colored plot of the percentage variations of the measured widths of the lines with respect to the nominal width.

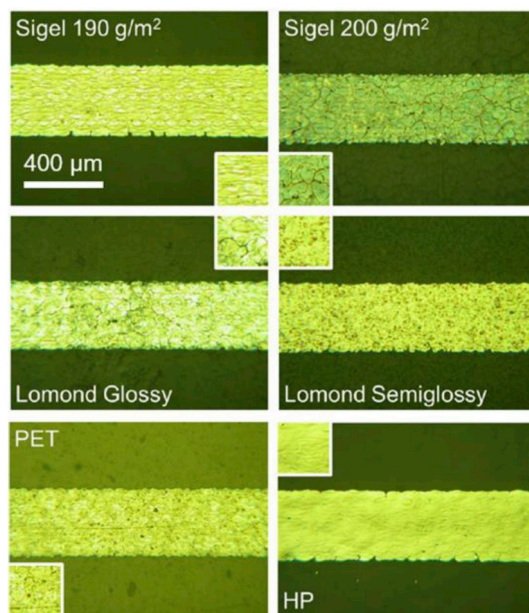


Fig. B4. Micrographs of 400 μm wide lines printed in the printhead's movement direction of different substrates.

Appendix C. Electrochemical sensors

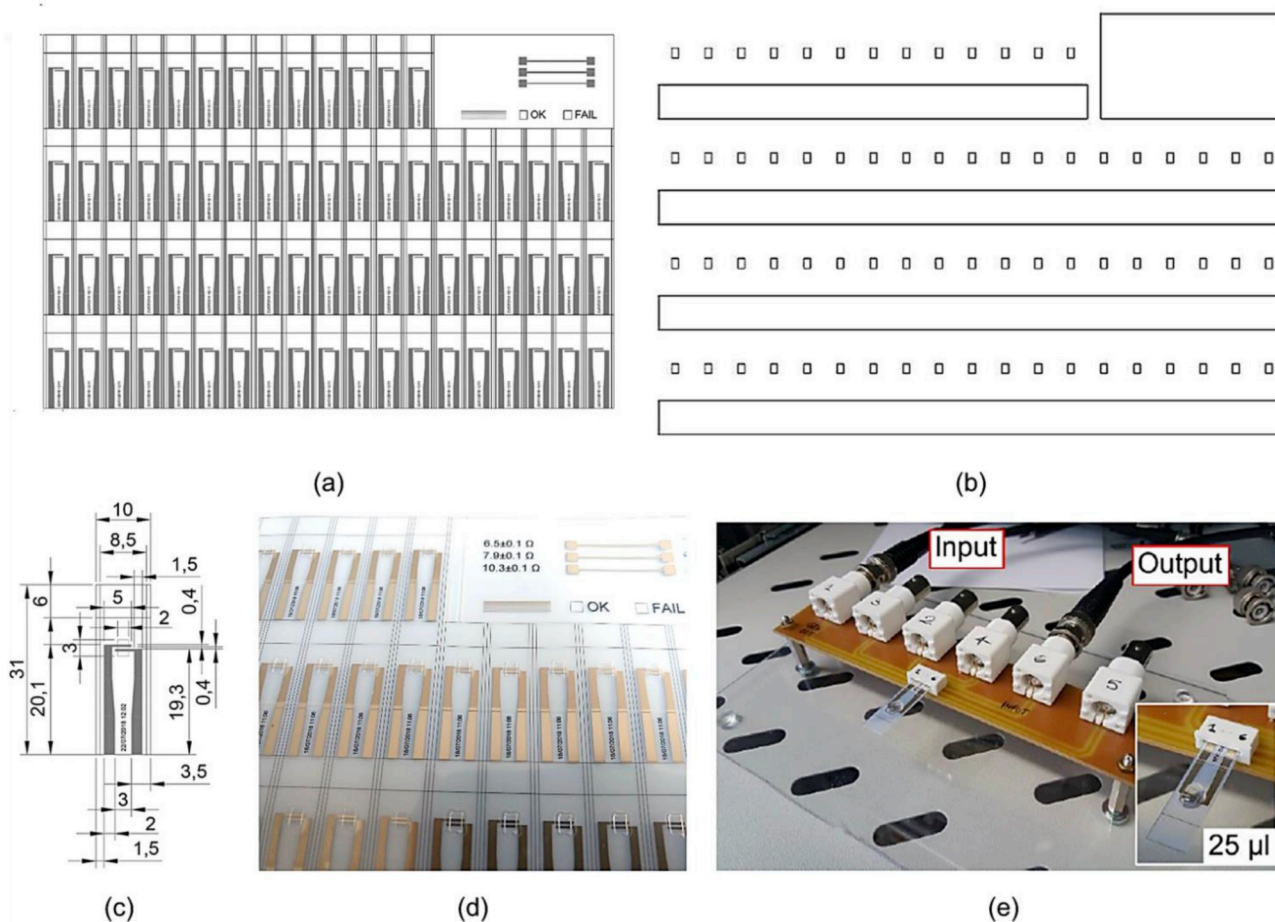


Fig. C1. (a) Printed sensors A5 sheet layout with printing quality control (top right part); (b) Plastic pouch cutting layout; (c) Dimensions of the designed sensors (in mm); (d) Picture of the printed and passivated sensors; (e) Test bench used for the EIS measurements.

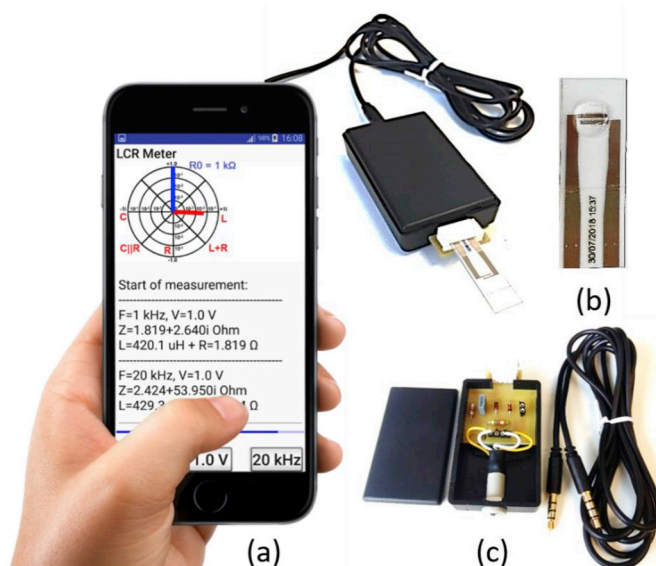


Fig. C2. Setup for the smartphone measurements (a), Sample device with testing solution on the interdigitated electrodes area (b), and hardware used for the EIS measurements through the smartphone headset (c).

This research did not receive any specific grant from funding agencies in the public, commercial, or not-for-profit sectors. All authors attest that they meet the current ICMJE criteria for Authorship. The authors have no financial disclosures.

References

- [1] M. Jung, et al., Based bimodal sensor for electronic skin applications, *ACS Appl. Mater. Interfaces* 9 (32) (2017) 26974–26982, <https://doi.org/10.1021/acsami.7b05672>.
- [2] Y. Wei, Y. Li, R. Torah, J. Tudor, Laser curing of screen and inkjet printed conductors on flexible substrates, *Symposium on Design, Test, Integration and Packaging of MEMS/MOEMS*, 2015, pp. 1–4, <https://doi.org/10.1109/DTIP.2015.7160991>.
- [3] M. Jović, et al., Inkjet-printed microtiter plates for portable electrochemical immunoassays, *J. Electroanal. Chem.* 786 (2017) 69–76, <https://doi.org/10.1016/j.jelechem.2016.12.051>.
- [4] H.K. Raad, H.M. Al-Rizzo, A.I. Abbosh, A.I. Hammoodi, A compact dual band polyimide based antenna for wearable and flexible telemedicine devices, *Prog. Electromagn. Res.* 63 (2016) 153–161, <https://doi.org/10.2528/PIERC16010707>.
- [5] S. Zhang, G. Wright, Y. Yang, Materials and techniques for electrochemical biosensor design and construction, *Biosens. Bioelectron.* 15 (2000) 273–282, [https://doi.org/10.1016/S0956-5663\(00\)00076-2](https://doi.org/10.1016/S0956-5663(00)00076-2).
- [6] L. Gonzalez-Macia, A. Morrin, M.R. Smyth, A.J. Killard, Advanced printing and deposition methodologies for the fabrication of biosensors and biodevices, *Analyst* 135 (2010) 845–867, <https://doi.org/10.1039/B916888E>.
- [7] H.-H. Lee, K.-S. Chou, K.-C. Huang, Inkjet printing of nanosized silver colloids, *Nanotechnology* 16 (2005) 2436, <https://doi.org/10.1088/0957-4484/16/10/074>.
- [8] H. Ma, Y. Su, C. Jiang, A. Nathan, Inkjet-printed Ag electrodes on paper for high sensitivity impedance measurements, *RSC Adv.* 6 (2016) 84547–84552, <https://doi.org/10.1039/C6RA18645A>.
- [9] J.T. Delaney, P.J. Smith, U.S. Schubert, Inkjet printing of proteins, *Soft Matter* 5 (2009) 4866–4877, <https://doi.org/10.1039/B909878J>.
- [10] L. Setti, A. Fraleoni-Morgera, I. Mencarelli, A. Filippini, B. Ballarin, M. Di Biase, An HRP-based amperometric biosensor fabricated by thermal inkjet printing, *Sens. Actuators B Chem.* 126 (2007) 252–257, <https://doi.org/10.1016/j.snb.2006.12.015>.
- [11] C. Ruan, L. Yang, Y. Li, Immunobiosensor chips for detection of *Escherichia coli* O157: H7 using electrochemical impedance spectroscopy, *Anal. Chem.* 74 (2002) 4814–4820, <https://doi.org/10.1021/ac025647b>.
- [12] G. Mattana, et al., Woven temperature and humidity sensors on flexible plastic substrates for e-textile applications, *IEEE Sens. J.* 13 (2013) 3901–3909, <https://doi.org/10.1109/JSEN.2013.2257167>.
- [13] N. Komuro, S. Takaki, K. Suzuki, D. Citterio, Inkjet printed (bio) chemical sensing devices, *Anal. Bioanal. Chem.* 405 (2013) 5785–5805, <https://doi.org/10.1007/s00216-013-7013-z>.
- [14] K. Yamada, T.G. Henares, K. Suzuki, D. Citterio, Paper-based inkjet-printed microfluidic analytical devices, *Angew. Chem. Int. Ed.* 54 (2015) 5294–5310, <https://doi.org/10.1002/anie.201411508>.
- [15] Z. Nie, et al., Electrochemical sensing in paper-based microfluidic devices, *Lab Chip* 10 (2010) 477–483, <https://doi.org/10.1039/B917150A>.
- [16] D. Tobjörk, et al., IR-sintering of ink-jet printed metal-nanoparticles on paper, *Thin Solid Films* 520 (2012) 2949–2955, <https://doi.org/10.1016/j.tsf.2011.10.017>.
- [17] S. Kumar, V. Bhat, K.J. Vinoy, V. Santhanam, Using an office inkjet printer to define the formation of copper films on paper, *IEEE Trans. Nanotechnol.* 13 (2014) 160–164, <https://doi.org/10.1109/TNANO.2013.2295765>.
- [18] A.P. Alves, J.F.A. Martins, H.P. da Silva, A. Lourenço, A.L.N. Fred, H. Ferreira, Experimental study and evaluation of paper-based inkjet electrodes for ECG signal acquisition, *PhysCS* (2014) 275–281, <https://doi.org/10.5220/0004720802750281>.
- [19] X. Nie, H. Wang, J. Zou, Inkjet printing of silver citrate conductive ink on PET substrate, *Appl. Surf. Sci.* 261 (2012) 554–560, <https://doi.org/10.1016/j.apsusc.2012.08.054>.
- [20] F. Molina-Lopez, D. Briand, N.F. De Rooij, All additive inkjet printed humidity sensors on plastic substrate, *Sens. Actuators B Chem.* 166 (2012) 212–222, <https://doi.org/10.1016/j.snb.2012.02.042>.
- [21] K. Crowley, et al., Fabrication of an ammonia gas sensor using inkjet-printed polyaniline nanoparticles, *Talanta* 77 (2008) 710–717, <https://doi.org/10.1016/j.talanta.2008.07.022>.
- [22] E. Song, T.H. da Costa, J.-W. Choi, A chemiresistive glucose sensor fabricated by inkjet printing, *Microsyst. Technol.* 23 (2017) 3505–3511, <https://doi.org/10.1007/s00542-016-3160-4>.
- [23] G. Rosati, M. Ravarotto, M. Scaramuzza, A. De Toni, A. Paccagnella, Silver nanoparticles inkjet-printed flexible biosensor for rapid label-free antibiotic detection in milk, *Sens. Actuators B Chem.* 280 (2019) 280–289, <https://doi.org/10.1016/j.snb.2018.09.084>.
- [24] and others, S. Kanchi, M.I. Sabela, P.S. Mdluli, K. Bisetty, Smartphone based bioanalytical and diagnosis applications: a review, *Biosens. Bioelectron.* 102 (2018) 136–149, <https://doi.org/10.1016/j.bios.2017.11.021>.
- [25] F. Li, Y. Bao, D. Wang, W. Wang, L. Niu, Smartphones for sensing, *Sci. Bull.* 61 (2016) 190–201, <https://doi.org/10.1007/s11434-015-0954-1>.
- [26] Z. Geng, X. Zhang, Z. Fan, X. Lv, Y. Su, H. Chen, Recent progress in optical biosensors based on smartphone platforms, *Sensors* 17 (2017) 2449, <https://doi.org/10.3390/s17112449>.
- [27] L.-J. Wang, Y.-C. Chang, R. Sun, L. Li, A multichannel smartphone optical biosensor for high-throughput point-of-care diagnostics, *Biosens. Bioelectron.* 87 (2017) 686–692, <https://doi.org/10.1016/j.bios.2016.09.021>.
- [28] B. Choi, H.J. Kang, H.G. Cho, J. Choi, Development and evaluation of the innovative smartphone interface bioelectrical impedance analyzer, *J. Med. Dev.* 7 (2013) 20935, <https://doi.org/10.1115/1.4024339>.
- [29] D. Zhang, et al., Smartphone-based portable biosensing system using impedance measurement with printed electrodes for 2, 4, 6-trinitrotoluene (TNT) detection, *Biosens. Bioelectron.* 70 (2015) 81–88, <https://doi.org/10.1016/j.bios.2015.03.004>.
- [30] R. Harder, A. Diedrich, J.S. Whitfield, M.S. Buchowski, J.B. Pietsch, F.J. Baudenbacher, Smart multi-frequency bioelectrical impedance spectrometer for BIA and BIVA applications, *IEEE Trans. Biomed. Circuits Syst.* 10 (2016) 912–919, <https://doi.org/10.1109/TBCAS.2015.2502538>.
- [31] D. Zhang, et al., Protein detecting with smartphone-controlled electrochemical impedance spectroscopy for point-of-care applications, *Sens. Actuators B Chem.* 222 (2016) 994–1002, <https://doi.org/10.1016/j.snb.2015.09.041>.
- [32] X. Wang, et al., Audio jack based miniaturized mobile phone electrochemical sensing platform, *Sens. Actuators B Chem.* 209 (2015) 677–685, <https://doi.org/10.1016/j.snb.2014.12.017>.
- [33] M. Berti, Prototyping of Innovative Biosensors by Inkjet Printing, M.S. thesis Ing. Inf. Dept., Univ. of Padua, Padua, Italy, 2018. <https://play.google.com/store/apps/details?id=ru.yukhlin.lcrmeterdemo&hl=en>.
- [34] <https://play.google.com/store/apps/details?id=ru.yukhlin.lcrmeterdemo&hl=en>.
- [35] G. Rosati, J. Daprà, S. Cherré, N. Rozlosnik, Performance improvement by layout designs of conductive polymer microelectrode based impedimetric biosensors, *Electroanalysis* 26 (2014) 1400–1408, <https://doi.org/10.1002/elan.201400062>.
- [36] G. Rosati, M. Scaramuzza, E. Pasqualotto, A. De Toni, C. Reggiani, A. Paccagnella, Modeling of SAM impedance onto gold and silver thin-film mass-produced electrodes and their use for optimization of lactic acid detection, *IEEE Trans. NanoBioscience* 15 (2016) 756–764, <https://doi.org/10.1109/TNB.2016.2616194>.